

Article

Geochemical Characteristics of Graptolite Shale in the Pingliang Formation of the Ordos Basin, China: Implications for Organic Matter, Thermal Evolution, and Hydrocarbon Reservoir

Fengjiao Li ^{1,2}, Zhengliang Huang ³, Xiaofeng Wang ^{1,2}, Xiaofeng Liu ⁴, Wenhui Liu ^{1,2,5}, Zhenghong Cai ³, Houyong Luo ^{1,2}, Qingtao Wang ⁶ and Dongdong Zhang ^{1,2,*}

¹ State Key Laboratory of Continental Dynamics, Northwest University, Xi'an 710069, China

² Department of Geology, Northwest University, Xi'an 710069, China

³ Research Institute of Exploration and Development, PetroChina Changqing Oilfield Company, Xi'an 710018, China

⁴ No. 1 Oil Production Plant of Changqing Oilfield Branch of CNPC, Yan'an 716000, China

⁵ Petroleum Exploration and Production Research Institute, SINOPEC, Beijing 100083, China

⁶ Guangzhou Institute of Energy Testing, Guangzhou 511447, China

* Correspondence: zhangdd@nwu.edu.cn



Citation: Li, F.; Huang, Z.; Wang, X.; Liu, X.; Liu, W.; Cai, Z.; Luo, H.; Wang, Q.; Zhang, D. Geochemical Characteristics of Graptolite Shale in the Pingliang Formation of the Ordos Basin, China: Implications for Organic Matter, Thermal Evolution, and Hydrocarbon Reservoir. *Energies* **2022**, *15*, 8238. <https://doi.org/10.3390/en15218238>

Academic Editor: Xianglu Tang

Received: 30 September 2022

Accepted: 2 November 2022

Published: 4 November 2022

Publisher's Note: MDPI stays neutral with regard to jurisdictional claims in published maps and institutional affiliations.



Copyright: © 2022 by the authors. Licensee MDPI, Basel, Switzerland. This article is an open access article distributed under the terms and conditions of the Creative Commons Attribution (CC BY) license (<https://creativecommons.org/licenses/by/4.0/>).

Abstract: Graptolite-rich shale is the main layer of shale gas resources in the southern marine sedimentary basin. Recently, shale gas resources were discovered in the Ordovician marine graptolite-rich strata in the Ordos Basin. The graptolite shale in the study area is different from the marine graptolite shale in the Yangtze plate in southern China, and further exploration is needed. This paper presents core samples of the graptolite-rich shale of the Pingliang Formation in the southwest Ordos Basin as research objects. The graptolite genus and graptolite shale characteristics were studied using core observation, electron microscopy, scanning electron microscopy, and geochemical analysis. We determined the role of the sedimentary environment and thermal maturation of graptolite shale in hydrocarbon formation and explored the possibility of hydrocarbon generation. Many graptolite epidermises provide buried organic matter. The quiet sea and low-energy marine environment create favorable conditions for preserving organic matter. The tectonic process resulted in the evolution stage in the oil generation window. Different types of pores formed the spaces of hydrocarbons. Therefore, the shale of the Pingliang Formation has shale oil exploration potential, which complements the shale gas in the northwestern margin of the basin, and provides new venues for shale oil and gas exploration in northern China.

Keywords: Pingliang formation; graptolite shale; biostratigraphy; shale oil and gas; geochemical characteristics

1. Introduction

Decades after the North American shale gas revolution [1–3], shale oil and gas, as unconventional resources, have become an important part of global oil and gas resources [4–6]. During the transition period from the Ordovician to Silurian, organic shale was widely deposited worldwide. For a long time, China's marine shale gas has only been found in the Sichuan Basin in the Yangtze plate, called the Wufeng Formation Longmaxi Formation shale [7–9]. In recent years, natural gas reservoirs and low-yield gas wells have been found continuously during exploration of the Changqing Oilfield in the Wulalike Formation on the western margin of the Ordos Basin. Two exploration wells have obtained industrial gas flows of $4 \times 10^4 \text{ m}^3/\text{d}$ and $22 \times 10^4 \text{ m}^3/\text{d}$ in the Wulalike Formation. The exploration results assist in solving the dilemma of insufficient shale gas resources in the northern marine basin. Later, shale oil was found in the exploration of the Pingliang Formation on

the southern margin of the basin. The western margin of the basin presents a pattern of oil in the south and gas in the north.

A good correlation exists between the sedimentary environment of graptolite-rich shale and the formation environment of shale gas [10–13]. The fine division of biostratigraphy is helpful for providing a more accurate stratigraphic division and correlation standard for shale gas production. According to the distribution characteristics of graptolite biostratigraphy, paleontologists have divided six favorable shale gas blocks in the Yangtze area, which have been proven by exploration [13]. Therefore, the identification of graptolite species and the attribution of graptolite belts in graptolite shale are particularly important [14]. Paleontologists use the method of graptolite biostratigraphy to study the Ordovician–Silurian and establish a high-resolution graptolite zone sequence, which provides a basis for the stratigraphic division and correlation of black graptolite-rich shale [13–19]. The graptolite shale deposited in this period is comparable with the Wufeng Formation–Longmaxi Formation graptolite shale in the Yangtze area where breakthroughs have been made in shale gas exploration. The depositional environment will affect the living conditions of graptolites and the preservation of remains, and the type of depositional environment is closely related to the living environment of graptolite organisms [20]. Therefore, different faunal assemblages have certain indications for the depositional environment.

Pyrite in sedimentary strata is mainly formed by two kinds of sulfate reduction: thermochemical sulfate reduction (TSR) and bacterial sulfate reduction (BSR). BSR occurs in relatively low temperature (from 0 °C to 60 °C to 80 °C) sedimentary water body and shallow burial diagenetic environment, while TSR occurs in a relatively high temperature (100 °C to 140 °C) hydrothermal environment of a deep burial diagenetic stage [21]. The pyrite of BSR origin is of great significance to the restoration of the ancient sedimentary environment [22]. With the participation of sulfate reducing bacteria, BSR can produce large sulfur isotope fractionation, but due to the complex reaction process, the sulfur isotope value of pyrite also has a large range distribution, usually negative [23,24]. However, TSR occurred in the late diagenesis period with a higher reaction temperature [25]. TSR refers to the reaction of sulfate with hydrocarbons, in which sulfate is reduced and gaseous hydrocarbons are oxidized [21,26]. Therefore, TSR reaction also reflects the generation of hydrocarbons. Pyrite of hydrothermal origin inherits the sulfur isotope composition of sulfate radical in the hydrothermal source area, and these sulfate radicals are likely to come from anhydrite in sediment or the re-oxidation of pyrite formed in a later closed environment. Pyrites of TSR origin generally have positive sulfur isotope values [27].

The graptolite shale of the Wufeng Formation–Longmaxi Formation in the Sichuan Basin has a high TOC and is of type I–II ‘kerogen’ [28]. The graptolite shale of the Pingliang Formation is different from the shale of the Wufeng Formation–Longmaxi Formation of the Upper Yangtze Platform in southern China and the Barnett shale of North America, and it is characterized by low organic matter abundance, variable maturity, and high carbonate mineral content [13]. Whether the Pingliang Formation can be used as a hydrocarbon source to supply shale gas with large reserves is still a concern. Predecessors have researched the source rock characteristics and hydrocarbon generation potential of the Pingliang Formation [29–33]. Previous studies have shown that the TOC of black shale in the lower member of the Pingliang Formation (Wulalike Formation) is generally 0.3–1.1% (average of 0.59%), and the organic matter abundance in local depressions is relatively high, with an average TOC of 0.86% [34–36]. The maturity is high, belonging to the mature/over mature window, and it is in the stage of effective gas generation. Simultaneously, the southern section of the western margin of the basin is shallowly buried due to thrust and nappe, resulting in the existence of local low-maturity samples [34–36].

The maturity of the organic matter reflects the degree of the thermal evolution of an area. The organic matter maturity of the Pingliang Formation as a whole is highly mature to over mature, and it is in the stage of effective gas generation [15–17]. Due to the complex structure of the southwest margin of the Ordos Basin, a large tectonic event occurred in the Late Ordovician, and it is described in detail in the geological background. Due to the

development and evolution of the central palaeo-uplift, the uplift of the southwest margin resulted in a lower degree of thermal evolution than that of the Pingliang Formation as a whole [37]. As the Pingliang Formation in this area is now buried below 3500 m, no detailed study on the degree of evolution has been conducted here. Recently, the Changqing Oilfield has drilled precious core samples; thus, the degree of geothermal evolution urgently needs to be studied. Vitrinite reflectance is considered to be the most reliable index for evaluating the maturity of organic matter. However, the Wulalike Formation lacks vitrinite, and the determination of its maturity has always been difficult when evaluating hydrocarbon source rocks. Previously, it was obtained by converting asphalt or vitrinite-like reflectivity into equivalent vitrinite reflectance [38–40]. In recent years, an increasing number of scholars have focused on the reflectivity of the graptolite epidermis [39,41–44]. The graptolite epidermis has strong anisotropy, and the nongranular graptolite epidermis has stronger anisotropy and higher random reflectivity than the granular graptolite epidermis. Previous studies have confirmed that the reflectivity of nongranular graptolite epidermis increases with increasing depth and has a logarithmic curve similar to the vitrinite reflectance–depth curve [45]. This shows that the reflectance of the graptolite epidermis, such as vitrinite reflectance, can reflect the response of organic matter to the effect of geothermal heating, and can also be used to characterize the maturity of organic matter. Compared with bitumen, the random reflectance of graptolite, as a thermal maturity parameter, has the advantages of being single origin, belonging to primary macerals, being large in quantity and easy to identify [46].

The graptolite-rich shale in the Pingliang Formation, as a reservoir of shale oil and gas, has been confirmed by exploration, and the microstructural characteristics of graptolite shale have been studied extensively [47]. Through scanning electron microscope observation, the biological structure of graptolite contributes to the development of primary pores in shale [28,48,49]. The characteristics of graptolite preserved along the plane lead to the development of microcracks [50]. Therefore, the contribution of graptolite to hydrocarbon generation potential and the enrichment and preservation of shale gas are of great significance.

In this paper, an organic geochemical analysis of the graptolite-rich shale in the Pingliang Formation of Well YT2 was conducted, and it was focused particularly on the maturity of organic matter. This study can supplement the geochemical study of source rocks in the southwest margin of Ordos Basin, and provide a basis for the exploration of shale oil and gas in the Pingliang Formation. Moreover, this study provides ideas for the breakthrough of global low TOC shale oil and gas exploration.

2. Geological Setting

The Ordos Basin is divided into six first-level structural units, including the western margin thrust belt, the Tianhuan depression, the Yishan slope, the Jinxi flexural fold belt, the Yimeng uplift, and the Weibei uplift (Figure 1A) [51]. The western structure of the Ordos Basin is complex, the tectonic activity of the western margin thrust belt is relatively strong, and the fault belt is developed, but the Tianhuan depression is relatively stable.

During the depositional period of the Pingliang Formation, the basin interior was uplifted, and differential subsidence occurred in the western region. Therefore, a set of bordered terrigenous sediments was formed, and the deep-water slope-shelf-basin facies sedimentary system developed from east to west [35]. Due to different stratigraphic naming systems in different areas of the Ordos Basin (Table 1), the lower part of the Pingliang Formation in the south of the western margin corresponds to the Wulalike Formation in the north, and the upper part corresponds to the Lashizhong Formation and Gongwusu Formation [52,53]. This study focuses on the lower part of the Pingliang Formation (Wulalike Formation). The lower part of the Pingliang Formation belongs to the strata deposited from the Middle Ordovician from the late Darrewell period to the Sambi period. Its TOC is higher than that in the upper part of the Pingliang Formation (Lashizhong Formation) [54–56]. The deep-water slope facies graptolite shale developed in

this formation is the main layer for shale gas exploration and development [54–57]. The Pingliang Formation shale is exposed at the surface in the Laoshidan section of Wuhai city in the north (called the Wulalike Formation and the Lashizhong Formation) and the Guanzhuang section of Pingliang in the south. The lithology is dominated by shale, calcareous mudstone, and dolomitic mudstone. The thickness of the stratum is 20–1200 m, and it gradually thickens from east to the west (Figure 1A) [34]. The southwest margin of the Ordos Basin is close to the Qilian–Qinling orogenic belt. In the middle and late Ordovician, due to the severe northward subduction of the Shangdan oceanic crust, the convergent plate margin was transformed into a back-arc basin of an extensional nature [29]. Due to the thrust nappe, the main part of the North China Craton, including the Ordos Basin, was uplifted and retreated, resulting in shallow burial of the strata, and even the outcropping of the surface, resulting in the loss of local strata at the southwest edge [58] and leading to the existence of local low-maturity samples. Research on shale of the Pingliang Formation shale in this area is still limited.

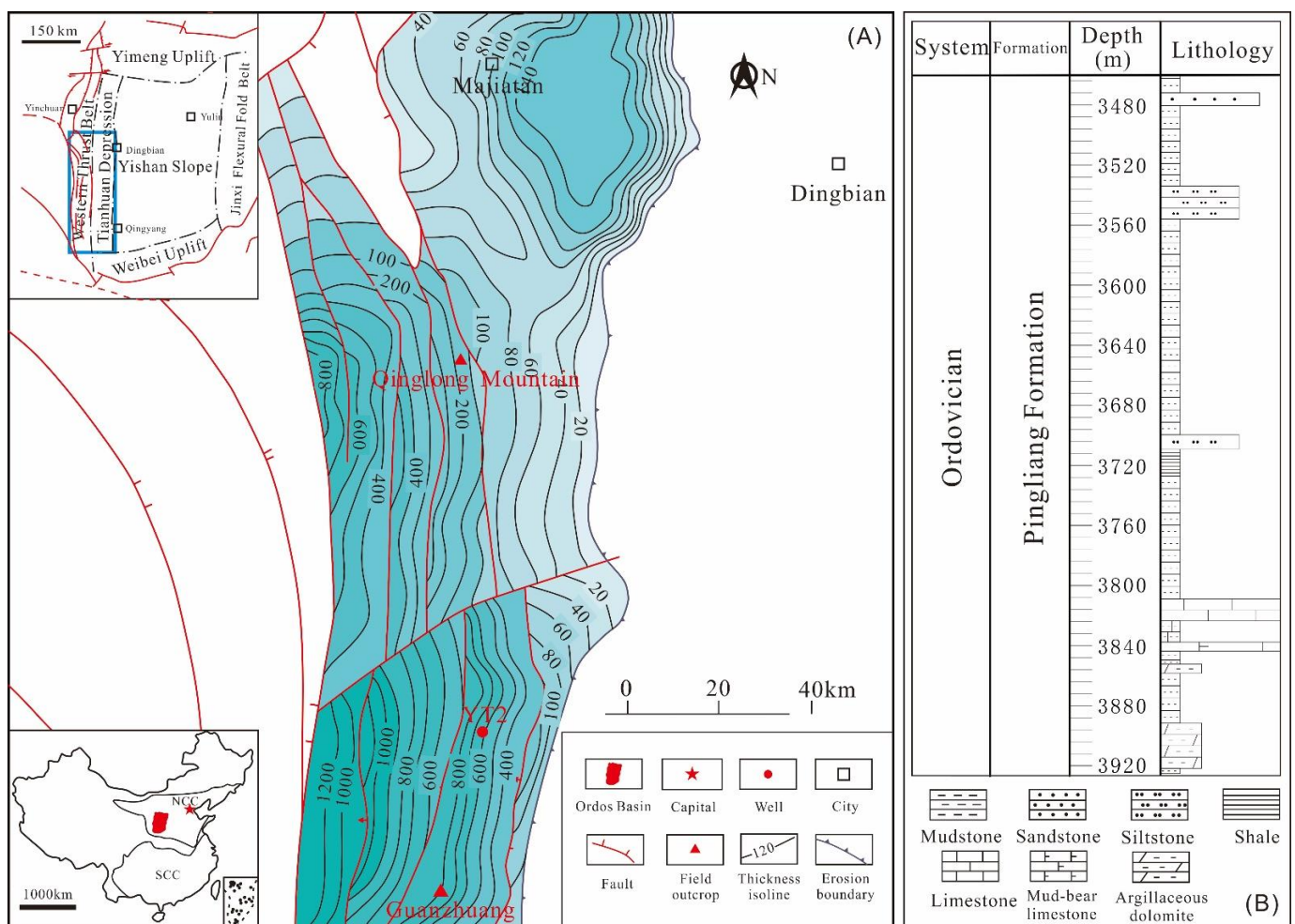


Figure 1. (A) Location and thickness map of the Wulalike Formation in the study area (according to [4]) (NCC: North China Craton, SCC: South China Craton); (B) the strata histogram.

Table 1. Stratigraphic correlation between the south and north of western Margins of Middle and Upper Ordovician in the Ordos Basin [52,53].

System	Series	Stage	South of Western Margin	North of Western Margin
Ordovician	Upper	Hirnantian	-	-
		Katian	Beiguoshan Formation	-
		Sandbian	Pingliang Formation	Gongwusu Formation Lashizhong Formation Wulalike Formation
	Middle	Darriwilian	Majiagou Formation	Kelimoli Formation
		Dapingian		Zhuozishan Formation

3. Samples and Methods

3.1. Samples

The seven drill core samples collected in this paper are from the lower part of the Pingliang Formation in Well YT2 in the southern segment of the western margin of the Ordos Basin (Figure 1B). The samples are mainly grayish black shale, distributed at depths of 3861–3871 m (Table 2), and graptolites are often found in core samples with bedding development. A diamond wire saw was used to cut the core samples into cylinders with a height of 4 cm and a diameter of approximately 10 cm. Part of the sample was consolidated with epoxy resin. Three blocks with a length of 3 cm, width of 2 cm, and height of approximately 0.5 cm were cut along the vertical and parallel bedding directions. Then, the core debris was randomly consolidated with epoxy resin to make blocks with a diameter of 2 cm and a height of 0.5 cm. All blocks were polished on an automatic lapping and polishing machine into light sheets for reflectance measurement. Another part of the sample was made into 1 × 0.5 × 0.5 cm cuboids and kept fresh for SEM analysis. The remaining samples were crushed into 120–200 mesh powder for geochemical analysis.

Table 2. Major element contents.

Sample	Depth(m)	SiO ₂ (%)	TiO ₂ (%)	Al ₂ O ₃ (%)	TFe ₂ O ₃ (%)	MnO (%)	MgO (%)	CaO (%)	Na ₂ O (%)	K ₂ O (%)	P ₂ O ₅ (%)	LOI (%)
YT2-1	3861.63	56.47	0.35	8.21	3.80	0.05	3.82	11.00	0.58	2.03	0.06	13.63
YT2-2	3862.21	59.99	0.45	12.02	4.39	0.03	3.08	6.55	0.71	3.14	0.09	9.55
YT2-3	3863.08	64.71	0.53	12.49	4.84	0.03	3.44	2.35	0.81	3.28	0.06	7.46
YT2-4	3864.41	51.27	0.44	12.77	4.51	0.04	4.83	8.73	0.70	3.36	0.06	13.29
YT2-5	3865.19	55.59	0.43	11.45	4.64	0.04	4.08	8.05	0.70	2.97	0.06	11.99
YT2-6	3868.93	62.65	0.49	11.95	4.54	0.03	3.15	4.60	0.80	3.14	0.07	8.58
YT2-7	3871.20	63.73	0.50	11.60	4.87	0.03	3.27	4.05	0.73	2.95	0.06	8.21

3.2. Methods

3.2.1. TOC and Rock-Eval

The TOC was obtained by a LECO CS744 carbon–sulfur analyzer. First, ~200 mg of the dried rock powder was accurately weighed into permeable crucibles. Second, excessive hydrochloric acid solution (HCl; volume HCl/volume water = 1:7) was added to samples, and the samples were kept at room temperature for 12 h and heated in a water bath at 80 °C for 3 h to remove carbonate minerals. Third, residues were diluted with distilled water to neutral pH and dried at 40 °C for 12 h for TOC measurement by a carbon–sulfur analyzer. The analytical precision was better than 0.1%. A rock pyrolysis analysis was performed at the Lanzhou Institute of Geology and Geophysics, Chinese Academy of Sciences. The rock samples were placed in a pyrolysis furnace and heated from room temperature to 550 °C at a certain heating rate (20 °C/min). S₁ is the free hydrocarbon (mg HC/g Rock), comprising the hydrocarbon products before heating to 300 °C in the heating process; S₂

is the cracked hydrocarbon (mg HC/g Rock), denoting the hydrocarbon products after 300 °C. T_{max} is the maximum pyrolysis peak temperature, which is the temperature with the highest hydrocarbon generation rate. The S_1 and S_2 precisions are better than 0.5 mg HC/g rock. The data validity of T_{max} is ± 2 °C.

3.2.2. GR_{ran}

The reflectance measurement process was completed on an optical microscope equipped with an optical microscope photometer. The reflectance of graptolite skin was measured under an oil immersion 50 times the objective lens with reflected light, and the measured reflectance of graptolite skin was random. The experiment was completed at the Laboratory of thermochronology, Department of Geology, Northwest University.

3.2.3. Major Elements

Major elements were analyzed by X-ray fluorescence spectrometry on a RIX2100 system. The loss on ignition (LOI) is the percentage weight lost after heating at 1000 °C for 2 h and cooling to 400 °C. Concentrations of major elements were analyzed with greater than 5% accuracy using a 1:5 ratio mixtures of dried sample powder and flux ($\text{Li}_2\text{B}_4\text{O}_7$). The above operating steps were in accordance with the China National Standard GB/T 14506.28-2010.

3.2.4. Sulfur Isotope Analysis of Pyrite

The pyrite sample was removed with a micro-sampler and weighed to a sulfur content of 60 μg in the tin capsules. The analysis was performed using a Thermo Scientific 253 Plus isotope ratio mass spectrometry (IRMS) system equipped with a Flash 2000HT Elemental Analyzer at 1020 °C. The generated SO_2 adopted the Chinese reference standard GBW04414 and was calibrated with the standard silver sulfide ($\delta^{34}\text{S} = -0.07\text{‰}$). All $\delta^{34}\text{S}_{py}$ data are reported relative to the VCDT scale, and the data accuracy was better than $\pm 0.5\text{‰}$.

3.2.5. Microscopic Observation

Samples were selected for microscopic observation by a Nikon Eclipse LV100N POL microscope. All observations were conducted under reflected light with a 50 \times oil immersion lens. The samples were coated with gold particles to increase their electrical conductivity before analysis by the scanning electron microscopy (SEM). SEM images were obtained on samples by a Thermo Fisher Helios G4 UC electron microprobe analyzer equipped with an SDD XMAX80 detector made by Oxford Instruments, Abingdon, UK. The chemical composition of minerals was measured at 10 kV and 0.4 mA with a resolution of 8 nm.

4. Results

4.1. Biostratigraphic Characteristics

The graptolites of the hand specimens were observed under a stereomicroscope and compared with the graptolite plate and feature description of the Ordovician Darivirian to Kaidian stage in Northwest China studied by Chen Xu [47], in order to identify the graptolite genus and species. According to the observation of hand specimens and the comparison with the paleontological plates, the 3861–3872 m section of well YT2 contains *Acrograptus eudiodus*, *Proclimograptus angustatus*, *Haddinggraptus oliveri*, *Dicranograptus kansuensis*, *Jiangxigraptus sextans*, and *Clinmagraptus bicornis* (Figure 2). Corresponding to the standard graptolite zone of the Pingliang Formation, all of the graptolite species found belong to the *Climacograptus bicornis* zone and *Nemagraptus gracilis* zone of the Pingliang Formation, corresponding to the Sambian of the Ordovician in international strata.

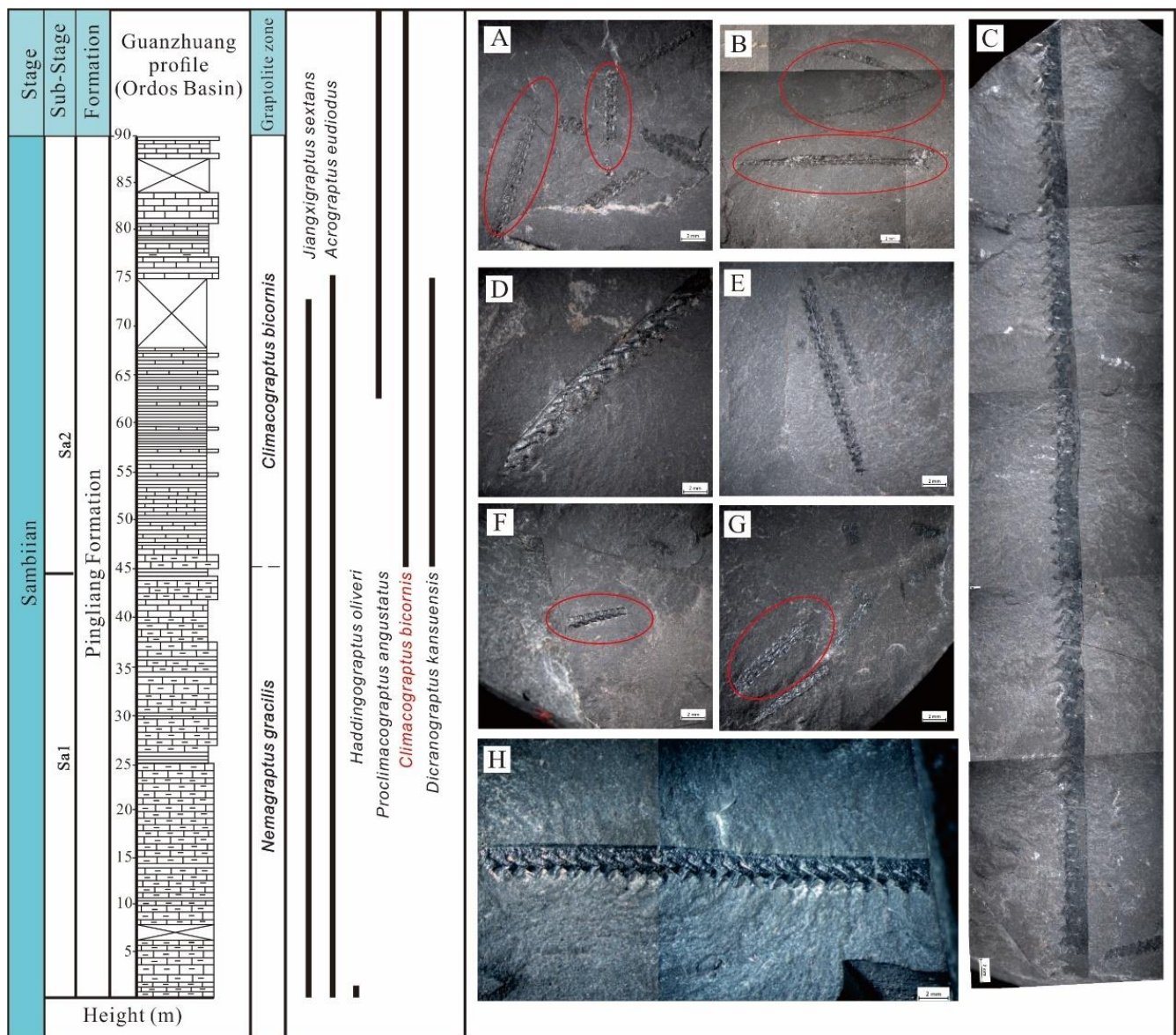


Figure 2. Graptolite extension map and characteristic photos in the study area (The scale bar is 2 mm.). (A) 3871.20 m, *Climacograptus bicornis*; (B) 3868.93 m, *Dicranograptus kansuensis*, *Proclimacograptus angustatus*; (C) 3865.19 m, *Acrograptus eudiodus*; (D) 3865.19 m, *Jiangxigraptus sextans*; (E) 3865.19 m, *Climacograptus bicornis*; (F) 3871.20 m, *Haddingograptus oliveri*; (G) 3865.19 m, *Climacograptus bicornis*; (H) 3865.19 m, *Acrograptus eudiodus*.

4.2. $\delta^{34}S_{py}$

The pyrite filling the graptolite epidermis is mainly strawberry pyrite, and the pyrite in the bedrock is mainly euhedral. The two types of pyrites were sampled by a microsampling instrument and subjected to sulfur isotope analysis. The results show two types of pyrite with different sulfur isotopic compositions: $\delta^{34}S_{py}$ filled in the graptolite cavity is -21.78‰ – -12.94‰ ; $\delta^{34}S_{py}$ in the bedrock is 11.84‰ – 25.86‰ .

4.3. Microstructural Characteristics of Graptolite Shale

As observed under the $50\times$ objective lens of the microscope oil immersion lens, the graptolites of the Wulalike Formation are dispersed in the black shale matrix in the form of carbonaceous film fragments, and the particle size of the carbonaceous film ranges from 10–100 μm (Figure 3A–D). Part of the graptolite cavity is filled with pyrite; thus, this part

of the graptolite epidermis is wrapped around pyrite (Figure 3E–I). In the parallel section, graptolite epidermis was produced in a lath (Figure 3A). Morphologically, the graptolite epidermis is divided into two types: nongranular graptolite epidermis and granular graptolite epidermis (Figure 3B,C). This phenomenon is consistent with previous research results [44,59]. The surface of the nongranular epidermis was smooth, and some of them showed an iconic spindle layer (Figure 3D). The surface of the granular epidermis is rough and can comprise particles of similar or different sizes under the microscope. Nongranular graptolite is mainly distributed in shale, granular graptolite is mainly distributed in carbonate rocks, and nongranular graptolite is mainly distributed in black shale of the Pingliang Formation [59]. On the parallel plane, the graptolite epidermis metasomatized by pyrite still retains a complete cell tube profile (Figure 3E). Under the microscope, the pyrite in the graptolite epidermis was observed to be present in two layers with different shapes, with a larger crystal form at the core and a smaller crystal form at the periphery (Figure 3F). Symmetrical shell residues are common in the vertical plane section (Figure 3G), and pyrite filling is more easily seen (Figure 3H,I). Pyrite fills the whole or part of the graptolite cavity.

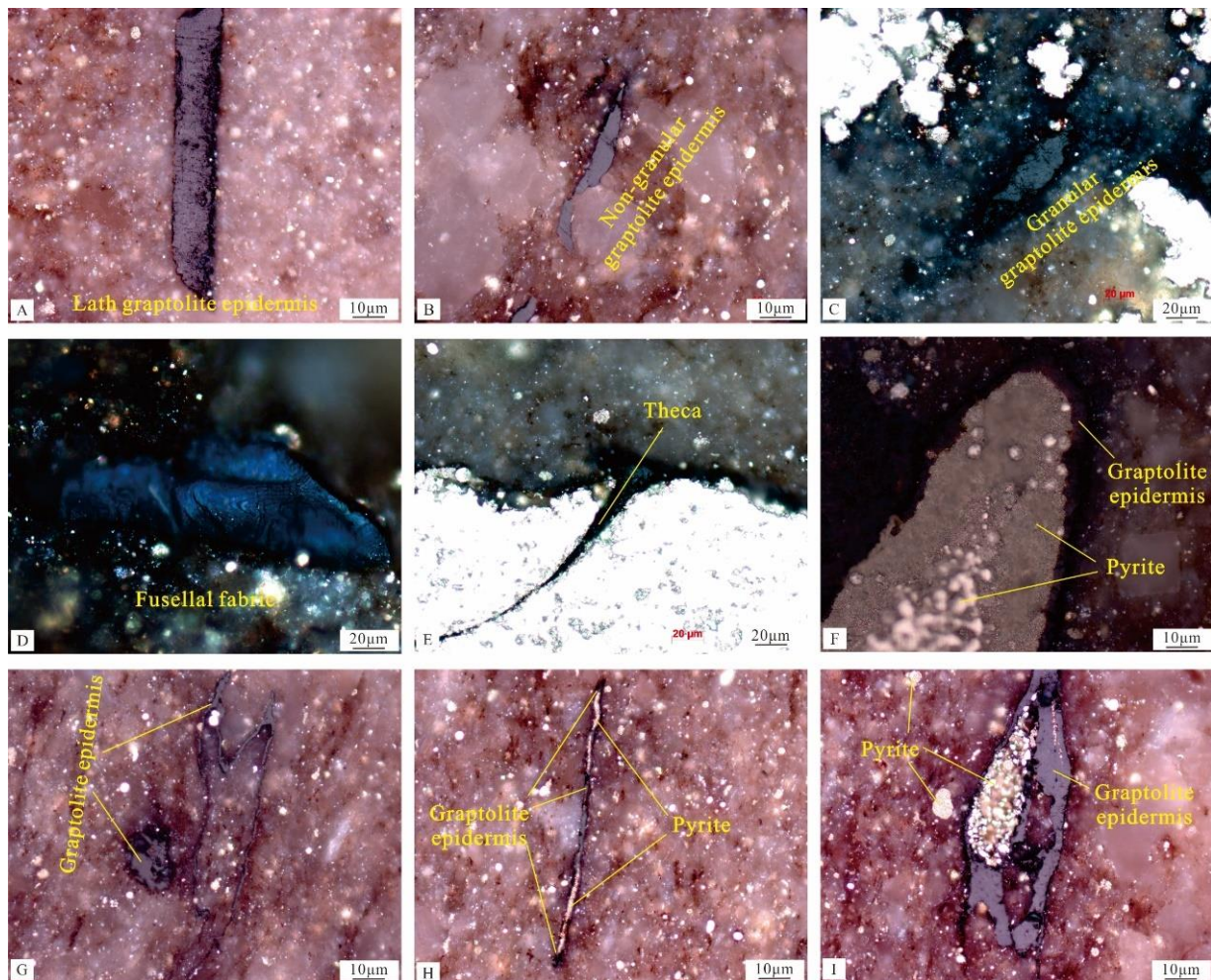


Figure 3. Characteristics of graptolite under the electron microscope. (A) lath graptolite epidermis, //, 3865.19 m; (B) nongranular graptolite epidermis, \perp , 3865.19 m; (C) granular graptolite epidermis, //, 3871.2 m; (D) fusellal fabric, //, 3868.93 m; (E) graptolite filled with pyrite retains the theca, //, 3871.2 m. (F) The graptolite cavity is filled with pyrite of different crystal forms. //, 3865.19 m; (G) graptolite epidermis on the vertical plane, \perp , 3865.19 m; (H) graptolite filled with pyrite, \perp , 3865.19 m; (I) graptolite partially filled with pyrite, \perp , 3865.19 m.

Under the scanning electron microscope, the graptolite epidermis is deposited in the bedrock with a carbonaceous film. After falling off, graptolite epidermis forms an impression on the bedrock, as shown in Figure 4A. The carbonaceous thin film exists in a layered structure. As shown in Figure 4B, the layered epidermis is loose, and pores formed by damage can be observed. The structure of the spindle layer in Figure 4C corresponds to the landmark spindle layer (Figure 3D) in the light sheet under the electron microscope. The graptolite epidermis is attached to the bedrock and filled with pyrite. The filled pyrite is strawberry pyrite (Figure 4D,E). The pyrite is mostly in a cluster shape, the crystal form of internal pyrite is small, and the crystal form of pyrite outside gradually becomes larger, and it is associated with dendritic clay minerals (Figure 4G); its composition is kaolinite based on energy spectrum analysis, as shown in Figure 5A. In the sample, the impression (Figure 4H) after strawberry pyrite shedding and the pores formed by pyrite particle shedding are often seen. Energy spectrum analysis shows that more than 85% of the impression composition is carbon (Figure 5B).

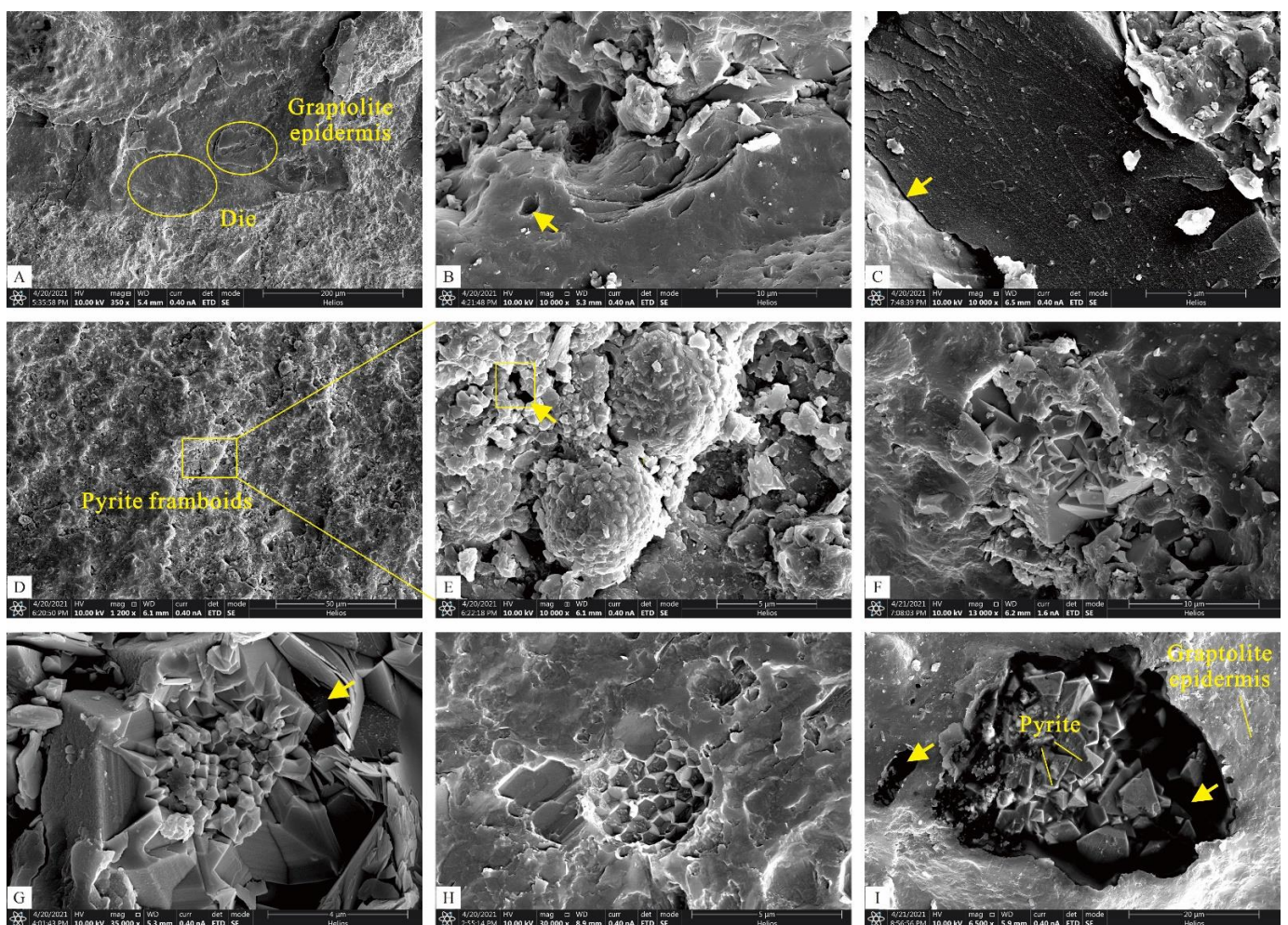


Figure 4. SEM image of graptolite shale. (A) layered structure and die of graptolite epidermis; (B) layered structure and organic pores of graptolite epidermis. The arrow points to the hole, and it is the same below; (C) fusellar fabric on the fresh section of graptolite epidermis and crevice; (D) large amount of pyrite framboids; (E) pyrite framboids and intergranular pores of pyrite; (F) euhedral pyrite. (G) Pyrite is associated with clay minerals and produces intergranular pores. (H) the impression on the graptolite epidermis after pyrite framboid removal; (I) graptolite cavity filled with pyrite.

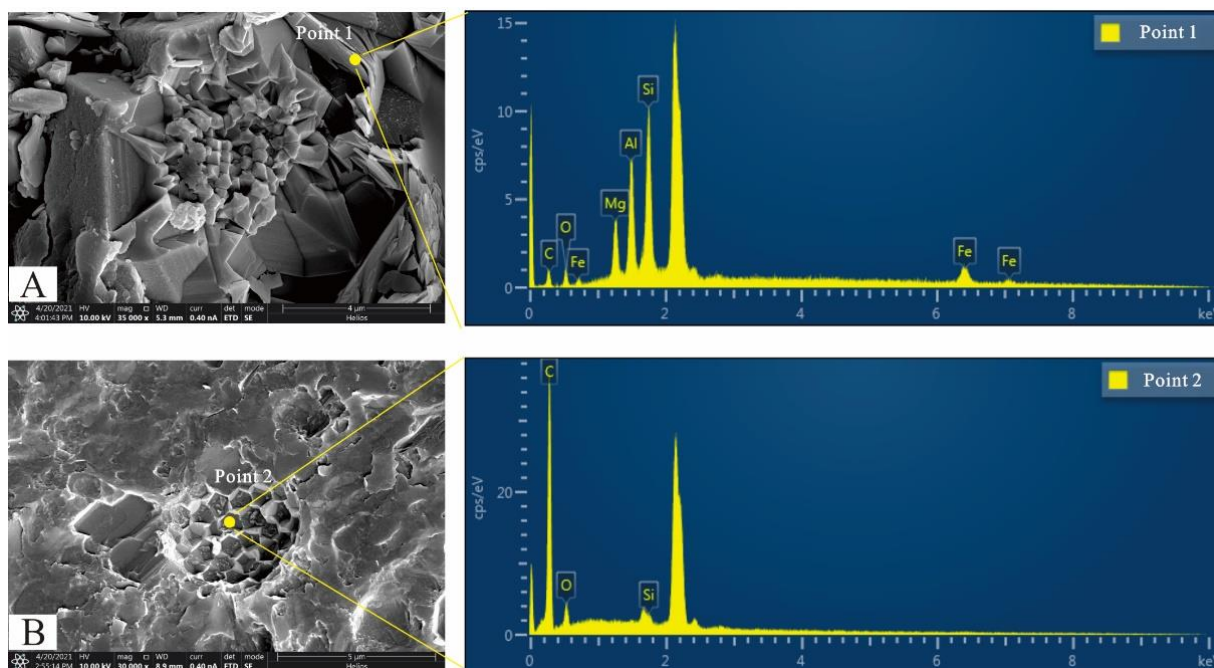


Figure 5. Energy spectrum image of graptolite shale. (A) The relationship between pyrite and clay minerals and energy spectrum of clay minerals. (B) The impression of pyrite on the graptolite epidermis and the energy spectrum of graptolite epidermis.

4.4. Major Element Contents

The major compounds analyzed in this study include SiO_2 , TiO_2 , Al_2O_3 , TFe_2O_3 , MnO , MgO , CaO , Na_2O , K_2O , and P_2O_5 (Table 2 and Figure 6). The concentrations of SiO_2 and Al_2O_3 are much higher than the concentrations of other major oxides. The average SiO_2 and Al_2O_3 contents of the shale from the Piangliang Formation are 59.2 and 11.5%, respectively, and are relatively stable.

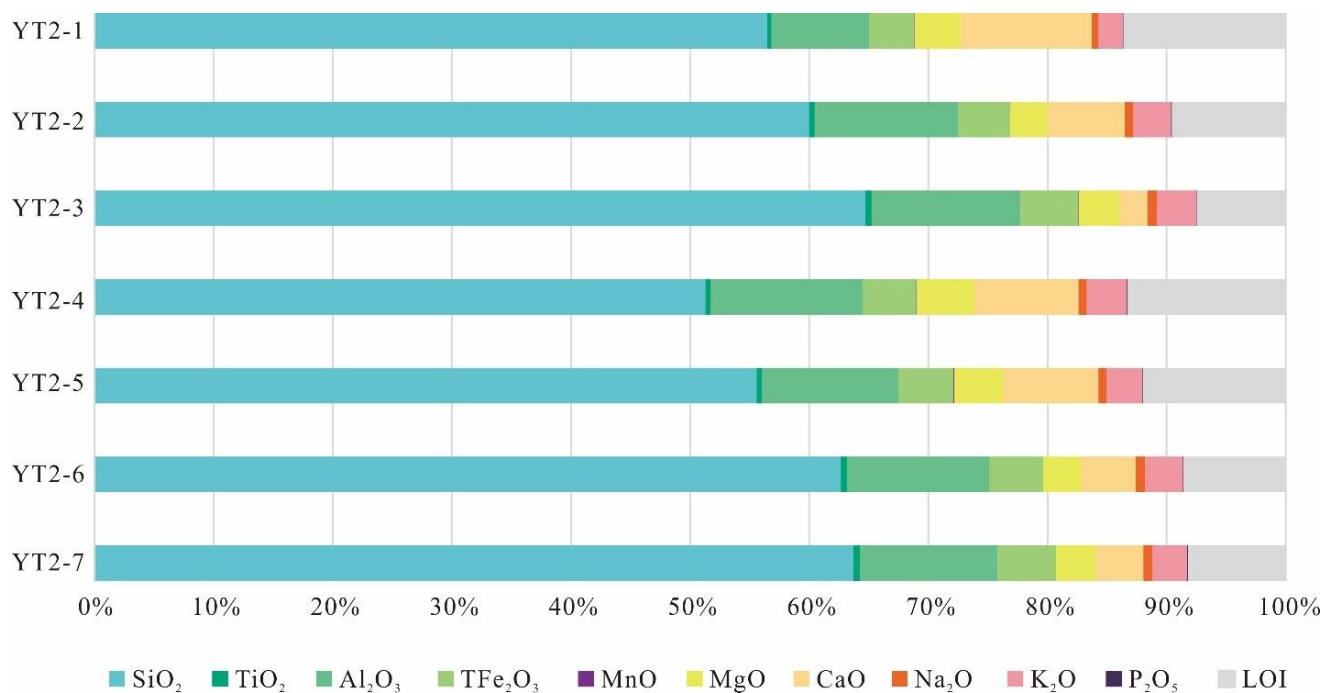


Figure 6. Diagram of major elements content.

4.5. Geochemical Characteristics of Graptolite Shale

The minimum TOC value of the tested samples was 0.31%, the maximum value was 0.93%, and the average value was 0.66% (Table 3). The rock pyrolysis data are shown in Table 2: S_1 is 0.36–0.50 mg HC/g Rock, S_2 is 0.99–1.14 mg HC/g Rock, $(S_1 + S_2)$ is 1.35–1.63 mg HC/g Rock, T_{max} is between 455–460 °C, and $PI = S_1/(S_1 + S_2)$ is 0.27–0.31 (Table 3).

Table 3. Rock pyrolysis analysis of black shale samples from the Wulalike Formation.

Sample	Depth (m)	TOC (%)	S_1	S_2	S_3	PI	T_{max} (°C)	HI	OI	Type
			(mg HC/g Rock)					(mg HC/g TOC)		
YT2-1	3861.63	0.58	/	/	/	/	/	/	/	/
YT2-2	3862.21	0.31	/	/	/	/	/	/	/	/
YT2-3	3863.08	0.65	/	/	/	/	/	/	/	/
YT2-4	3864.41	0.53	/	/	/	/	/	/	/	/
YT2-5	3865.19	0.93	0.50	1.12	0.33	0.31	456	121	36	II
YT2-6	3868.93	0.76	0.36	0.99	0.28	0.27	456	131	37	II
YT2-7	3871.20	0.86	0.49	1.14	0.40	0.30	459	155	54	II

The measured random reflectance of the graptolite epidermis of the Pingliang Formation in the Ordos Basin is concentrated between 1.00% and 1.26% (Table 4, Figure 7A). The equivalent vitrinite reflectance conversion formula of Cao et al. (2000) [60] and Luo et al. (2018) [44] was selected to convert the graptolite epidermis reflectance in the graptolite shale of the Pingliang Formation. The results are shown in Table 4. $EqVR_o^*$ is distributed in the range of 0.99–1.26%, which is nearly consistent with the random reflectance of graptolite epidermis (Table 4, Figure 7B). $EqVR_o^{**}$ is mainly distributed in the range of 1.03–1.08% (Table 4, Figure 7C).

Table 4. Calibration of sample maturity.

Sample	Slice Direction	Depth(m)	GR_{ran} (%)	Number of Measuring Points	$EqVR_o^*{}^1$	$EqVR_o^{**}{}^2$
YT2-1-1//	//	3871.2	0.74	65	0.73	0.883
YT2-1-2//	//	3871.2	1.04	40	1.05	1.07
YT2-1-3//	//	3871.2	1.07	67	1.08	1.09
YT2-2-1//	//	3868.93	1.21	60	1.23	1.17
YT2-2-2//	//	3868.93	1.22	60	1.23	1.17
YT2-3-1//	//	3865.19	1.22	60	1.23	1.17
YT2-1-1⊥	⊥	3871.2	1.01	60	1.01	1.06
YT2-1-2⊥	⊥	3871.2	1.14	60	1.14	1.13
YT2-1-3⊥	⊥	3871.2	1.01	60	1.01	1.06
YT2-2-1⊥	⊥	3868.93	1.33	60	1.35	1.24
YT2-2-2⊥	⊥	3868.93	1.44	60	1.46	1.29
YT2-2-3⊥	⊥	3868.93	1.49	60	1.52	1.32
YT2-3-1⊥	⊥	3865.19	1.13	60	1.14	1.13
YT2-3-2⊥	⊥	3865.19	0.90	60	0.89	0.99
YT2-3-3⊥	⊥	3865.19	0.95	60	0.95	1.02
YT2-1	Random	3871.2	1.09	38	1.09	1.10
YT2-2	Random	3868.93	1.201	32	1.21	1.17
YT2-3	Random	3865.19	0.85	36	0.84	0.96

¹ $EqVR_o^* = 1.055 \times GR_{ran} - 0.053$ [44]. ² $\lg EqVR_o^{**} = 0.572 \lg GR_{ran} + 0.021$ [60]. “//” indicates parallel to bedding plane. “⊥” indicates perpendicular to bedding plane.

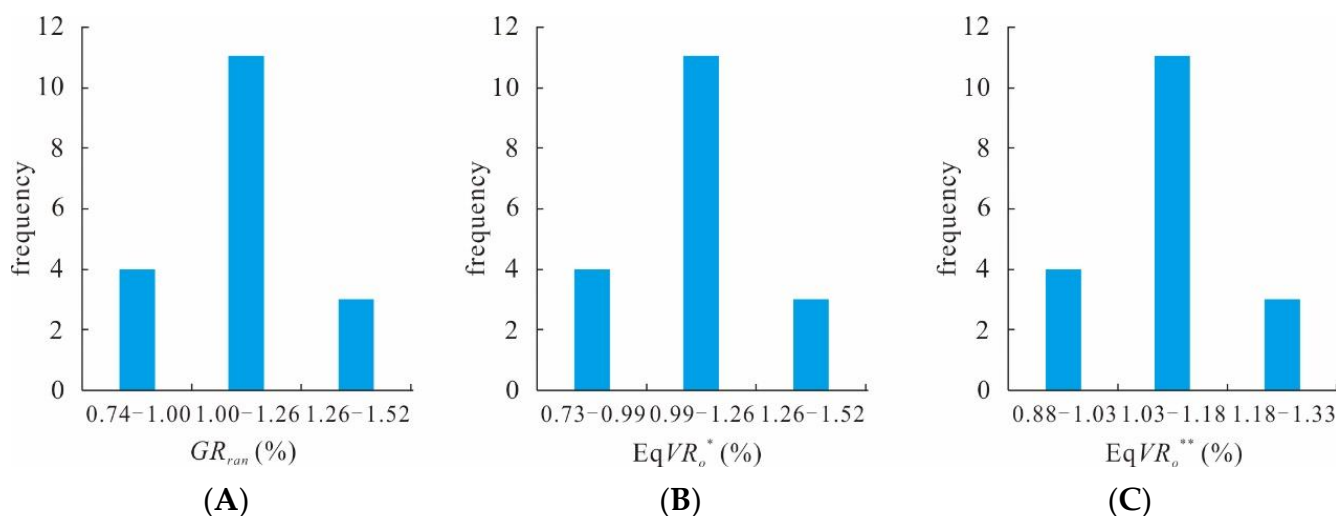


Figure 7. Random reflectance of graptolite and equivalent vitrinite reflectance distribution. (A) random reflectance of graptolite; (B) equivalent vitrinite reflectance distribution (according to [44]); (C) equivalent vitrinite reflectance distribution (according to [60]).

5. Discussion

5.1. Origin of Organic Matter in Graptolite Shale

The TOC of the samples in the study area range from 0.31–0.93% (average value: 0.66%). ($S_1 + S_2$) is 1.35–1.63 mg HC/g Rock. According to the classification standard of the source rock, this area is a poor source rock. However, some scholars have suggested that TOC is the residual carbon content, and the evaluation of source rocks should not be based on TOC alone [61]. In China, some scholars have proposed the subsistence of organic acid salts [62–64]. In the traditional TOC measurement method, this part of the material is lost in the pretreatment, which leads to the underestimation of hydrocarbon generation potential in the evaluation of source rocks [65]. Moreover, the types of hydrocarbon generating parent materials lead to differences in hydrocarbon generation conversion rates [66]. According to the HI and T_{max} of rock pyrolysis, the organic matter types of source rocks in the study area are divided. The kerogen of the source rocks in the study area is type II.

The graptolite epidermis is the most important organic component in the graptolite-rich shale of the Pingliang Formation in the Ordos Basin. Although the volume of graptolite epidermis is small, the quantity is large. The contribution of the graptolite epidermis to hydrocarbon generation is a controversial subject. Energy spectrum analysis shows that the carbon content of graptolite epidermis accounts for more than 80%, even up to 90%, which contributes to most of the carbon sources in graptolite-rich shale. According to the statistics of some scholars, graptolite epidermis accounts for 20–93% of the volume of dispersed organic matter in rocks, indicating that the graptolite epidermis is an important contribution to buried organic carbon [49]. The high TOC shale intervals in the Pingliang Formation of the Ordos Basin and the Longmaxi Formation of the Silurian in the Sichuan Basin correspond to the intervals with high graptolite abundance, indicating that graptolite has an important contribution to buried organic matter [23,67]. The TOC of black shale from the Wufeng Formation to the Longmaxi Formation has an obvious positive correlation with graptolite diversity. The pyrolysis data of single graptolite also show that residual organic carbon of graptolite is one of the important contributors to the organic carbon of black shale from the Wufeng Formation to the Longmaxi Formation [68]. In summary, graptolite organic matter plays an important role in hydrocarbon generation.

5.2. Indication of Graptolite Shale in Original Organic Matter Preservation

The sedimentary environment affects the basic living conditions and preservation conditions of graptolite, and the type of sedimentary environment is closely related to the

living environment of graptolite organisms [69]. Therefore, different faunal combinations can indicate corresponding sedimentary environments. Graptolite sank to the sea floor after death and was buried together with specific brachiopod assemblages [70]. Therefore, these specific brachiopod benthic assemblages (BAs) can indicate the seawater depth when graptolite assemblages (GAs) were buried together. Although no specific brachiopod assemblage has been found in the Ordovician, predecessors have determined the specific sedimentary environment of different graptolite genera and species according to the biological assemblage. Therefore, according to graptolite characteristics and specific global common burial assemblages, the depth zoning pattern of graptolite can be a reference (Figure 8) [71,72]. Many diallel graptolites occur in the study area. In the study area, the graptolite genera and species from the *Climacograptus bicornis* zone to the *Nemagraptus gracilis* zone in the study area include *Proclimacograptus angustatus*, *Haddingograptus oliveri*, *Dicranograptus kansuensis*, and *Climacograptus bicornis*. In terms of diversity and richness, they exceed the single row graptolite, such as the quiet *Acrograptus eudiodus* and *Jiangxigraptus sextans*. The diallel graptolite structure has better structural strength and can adapt to certain hydrodynamic strengths of surface water. It represents GA3, and its corresponding water depth is approximately 30–60 m. The single-row graptolite fauna can sink from the surface water to the deeper water, representing GA4-5. The corresponding water depth should be more than 100 m, but not more than 200 m. In the study area, graptolites from the *Climacograptus bicornis* zone to the *Nemagraptus gracilis* zone correspond to GA 3 and GA 4-5 in the graptolite depth zoning pattern, indicating that the early Pingliang period, that is, the Wulalike period, was a relatively deep-water sedimentary environment.

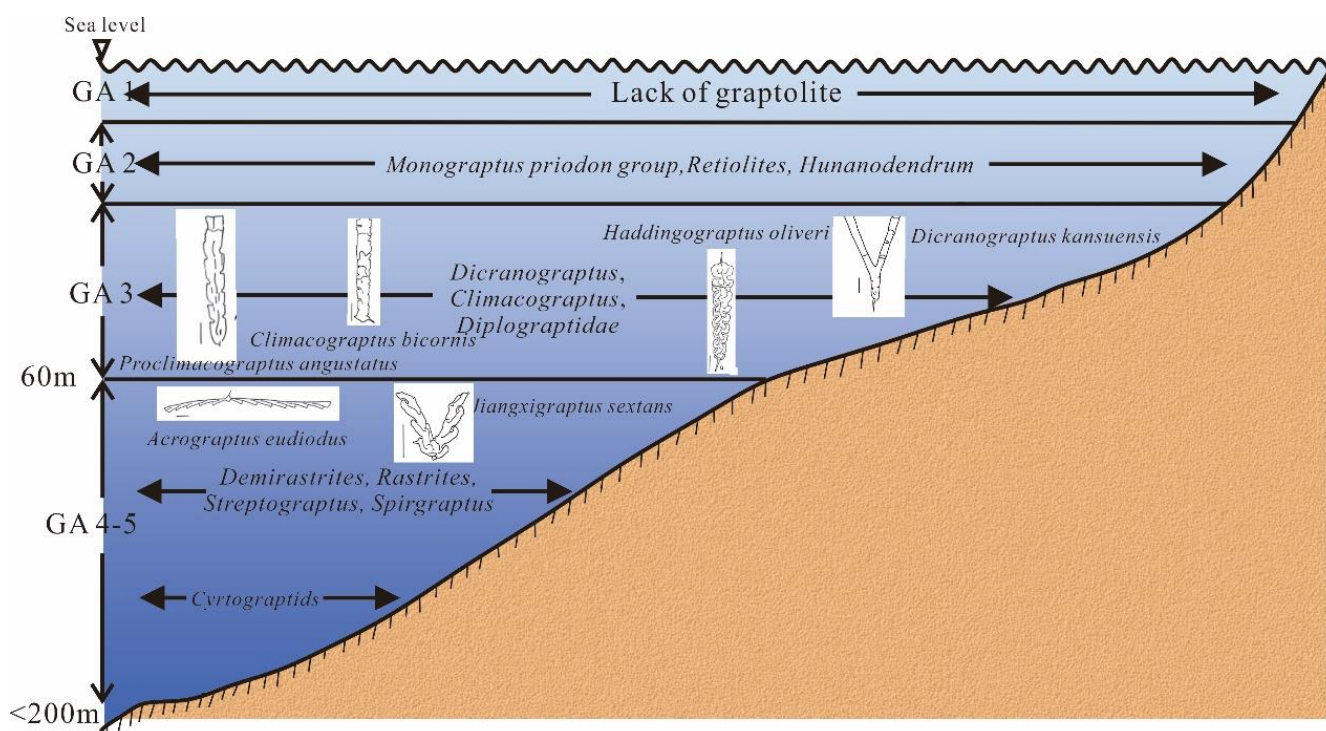


Figure 8. Depth zoning pattern of graptolites (according to [71,72]).

The deposition rate of deep-sea water is still slow, and fine-grained sediments hinder the circulation of the oxygen-rich water bodies and anoxic water bodies below. Moreover, H_2S produced by the decomposition of graptolitic remains difficult to diffuse, which leads to a reducing environment. In addition, H_2S combines with the iron element in the water to form pyrite. Furthermore, a reducing environment inhibits the survival of benthic organisms and avoids disturbing graptolitic remains. $\delta^{34}S_{py}$ and the occurrence characteristics of pyrite reflect the formation environment and later evolution process of shale [73]. The $\delta^{34}S_{py}$ and pyrite morphologies within the graptolite cavity suggest that the pyrite origin is

BSR. During the synsedimentary period, BSR occurred by active microorganisms under sulfur and iron enrichment conditions. The sedimentary environment is beneficial to the enrichment and preservation of organic matter. The mechanical damage by the water body is weak, and the graptolites are preserved and deposited in the shale layer. The distribution and preservation status of graptolites and the performance of sulfur isotopes reflect the low-energy, anoxic deep-water depositional environment.

The Ordovician paleogeographic features of the basin have been studied by others [74]. Studies have also been conducted on the sedimentary characteristics of the Early Pingliang Period (Wulalike Period) in the central western margin of the basin [75]. In the Guanzhuang section in the southern part of the western margin where the study area is located, some phenomena representing deep-water deposition were also observed. The Guanzhuang section comprises thin layers of marl and calcareous mudstone. It contains many graptolite-rich shale interlayers (Figure 9) and typical deep-water slope deposits.

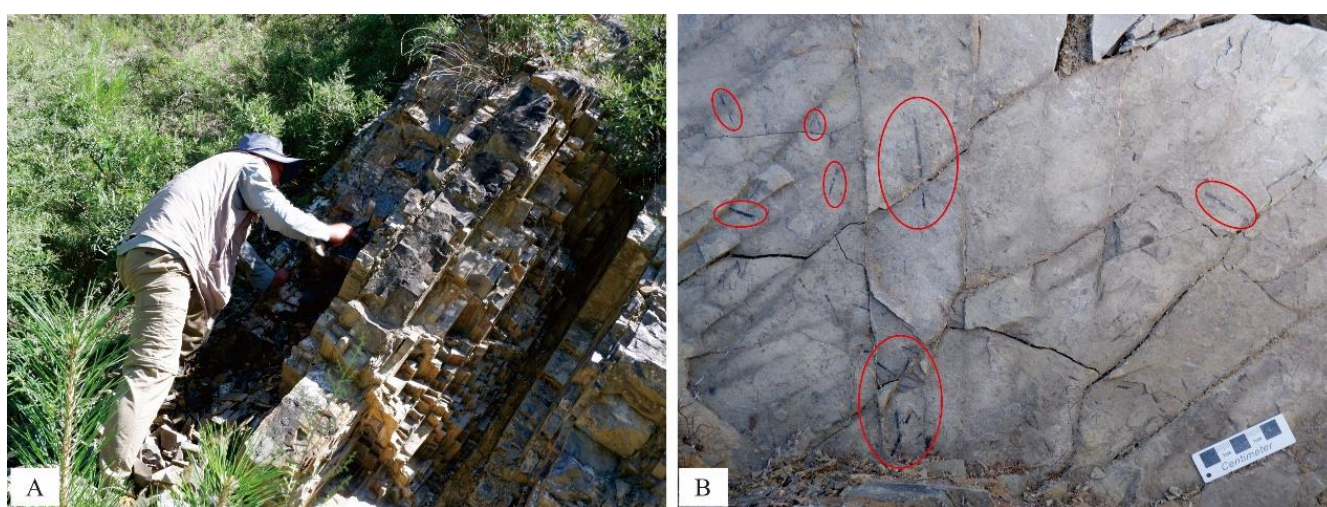


Figure 9. (A) Lithological association of the Pingliang Formation in the Guanzhuang section; (B) graptolite shale of the Pingliang Formation in the Guanzhuang section (In the red circles are graptolites.).

5.3. Indication of Graptolite Shale in Evolutionary Processes

The $\delta^{34}S_{py}$ and pyrite morphologies in the bedrock show completely different behaviors from those of the pyrite in the graptolitic cavity, which is typical of a TSR origin. This finding indicates that this depositional period may have been influenced by hydrothermal action. The high organic matter content and the significant burial depth of the Pingliang Formation provide potential conditions for the occurrence of TSR. The major reason for TSR is probably volcanic activity with a minor amount of hydrocarbons from shale maturation. Multiple layers of tuff interlayers in the lower part of the Pingliang Formation have also been observed in the Guanzhuang profile (Figure 10). This result shows multiple volcanic activities in this period, which also provided conditions for the occurrence of TSR in this area.

According to the identical vitrinite reflectance converted from graptolite reflectance, the equivalent vitrinite reflectance of black graptolite-rich shale of the Pingliang Formation in the research area of the southwest margin of Ordos is concentrated between 0.99% and 1.26%, which falls in the early stage of plutonic pyrolysis, that is, the oil generation window. The rock pyrolysis results show that T_{max} is between 455 °C and 460 °C, indicating that the shale of the Pingliang Formation has reached the mature stage. PI is also a commonly used maturity parameter. In the samples in this paper, the productivity index (PI) of graptolite shale in the Pingliang Formation was 0.27–0.31. The evaluation results of PI indicate that the hydrocarbon generation potential of black shale samples in the lower member of the Pingliang Formation has been moderately transformed into oil and gas, indicating the early evolution stage of maturity. The equivalent vitrinite reflectance combined with T_{max} and PI

indicates that the source rocks in this area are in the mature stage. The southern part of the western margin of the basin is subject to thrust napping, resulting in shallow burial of the strata; some samples have relatively low maturity [53]. This result will affect the overall resource evaluation of Pingliang Formation shale. Light oil appeared in adjacent wells, consistent with the thermal maturity of the study area.



Figure 10. (A) Multilayer tuff in the Pingliang Formation Guanzhuang section; (B) the upper layer is marl and the lower layer is tuff of the Pingliang Formation Guanzhuang section. The red lines indicate boundaries between tuff and shale, and the arrows point to layers of tuff.

5.4. Indication of Graptolite Shale in Hydrocarbon Reservoir Pore

The Pingliang Formation shale has been demonstrated to be a reservoir by exploration. Industrial gas flow has been successfully obtained in the north and light oil has been drilled in the south. Pore structures of different scales were observed in the study area in the graptolite-rich shale of the Pingliang Formation.

First, a number of primary organic pores were observed, and the primary pores were closely related to the biological structure of graptolite. Organic pores have developed on the graptolite epidermis. The horizontal bedding of the graptolite-enriched layer plays the role of hydrocarbon reservoir pore space and permeability pathways. Second, as the sedimentary environment controls graptolite-bearing shale, graptolite has been deposited and preserved along the bedding plane. Graptolite-rich laminar structures develop rich interlayer fractures, providing a certain reservoir space and gas seepage channels, thus improving the oil and gas storage and migration capacity of the shale. The graptolite shale of the Pingliang Formation also develops microfractures of different scales, which are developed to different degrees between and within crystals. The microfractures play a positive role in extending artificial fractures in the later development stage. Third, as observed under the scanning electron microscope, the cavity of the graptolite epidermis is filled with pyrite grains, and the grains gradually decrease in size and are arranged closely from the inside to the outside due to the restriction of growth space. Intergranular pores of nanometer-scale minerals have developed in pyrite grains. In addition, clay minerals are filled between the pyrite and graptolite skins, and the contact between pyrite and clay minerals also increases the number of intergranular pores. In summary, the different types of pores and adsorption of organic matter on oil and gas provide conditions for the accumulation of shale gas in the Pingliang Formation.

6. Conclusions

This study closely followed the exploration focus, determined the role of the sedimentary environment and thermal maturity evolution of graptolite shale in the formation of oil and gas, and discussed the possibility of oil and gas generation. The main points are as follows:

- (1). Graptolite epidermis is the primary carbon source in graptolite-rich shale. The geochemical characteristics of graptolite shale show that the TOC of this section meets the standard of hydrocarbon source rock, and the kerogen is type II.
- (2). The types of graptolites, pyrite manifestations, and field observations all show that this area is a deep-water, quiet sea sedimentary environment conducive to preserving organic matter.
- (3). The presence of pyrite and tuff in the section indicates that TSR have occurred in this area. Under the influence of tectonic activity, the degree of evolution of this area is within the oil-generating window.
- (4). Different types of pores are found in graptolite-rich shale, and they provide storage space for the occurrence of hydrocarbons in the Pingliang Formation.

Due to the “four in one” condition of buried organic matter, preservation, thermal evolution degree, and storage space, the Pingliang Formation has shale oil exploration potential, which complements the shale gas of the Wulalike Formation in the area north of the western margin of the basin, providing potential for shale oil and gas exploration in northern China. Moreover, this study provides ideas for the breakthrough of global low TOC shale oil and gas exploration.

Author Contributions: Writing—original draft preparation, review, and editing, F.L.; sample and methodology, D.Z., Z.C., Q.W. and X.L.; funding acquisition, W.L., X.W. and H.L.; investigation, Z.H. All authors have read and agreed to the published version of the manuscript.

Funding: This research was funded by the National Natural Science Foundation of China (Grant No. 41930426; No. 41972134; No. 42172173) and Major special projects of Changqing Oilfield (ZDZX2021-03).

Data Availability Statement: The data presented in this study are available on request from the corresponding author.

Acknowledgments: We sincerely appreciate editors and four reviewers for their constructive comments and assistance on this manuscript. We are grateful for the thoughtful suggestions from Xiaofu Li and Xiaoyan Chen during the revision of this manuscript.

Conflicts of Interest: The authors declare that they have no conflict of interest.

References

1. Montgomery, S.L.; Jarvie, D.M.; Bowker, K.A.; Pollastro, R.M. Mississippian Barnett shale, Fort Worth basin, north-central Texas: Gas-shale play with multi-trillion cubic foot potential. *AAPG Bull.* **2005**, *89*, 155–175. [[CrossRef](#)]
2. Sun, C.X.; Nie, H.K.; Dang, W.; Chen, Q.; Zhang, G.R.; Li, W.P.; Lu, Z.Y. Shale gas exploration and development in China: Current status, geological challenges, and future directions. *Energy Fuels* **2021**, *35*, 6359–6379. [[CrossRef](#)]
3. Dang, W.; Zhang, J.C.; Tang, X.; Wei, X.L.; Li, Z.M.; Wang, C.H.; Chen, Q.; Liu, C. Investigation of gas content of organic-rich shale: A case study from lower permian shale in southern north China basin, central China. *Geosci. Front.* **2018**, *9*, 559–575. [[CrossRef](#)]
4. Yang, F.; Xu, S.; Hao, F.; Hu, B.Y.; Zhang, B.Q.; Shu, Z.G.; Long, S.Y. Petrophysical characteristics of shales with different lithofacies in Jiaoshiba area, Sichuan Basin, China: Implications for shale gas accumulation mechanism. *Mar. Petrol. Geol.* **2019**, *109*, 394–407. [[CrossRef](#)]
5. Xu, S.; Gou, Q.Y.; Hao, F.; Zhang, B.Q.; Shu, Z.J.; Wang, Y.Y. Multiscale faults and fractures characterization and their effects on shale gas accumulation in the Jiaoshiba area, Sichuan Basin, China. *J. Pet. Sci. Eng.* **2020**, *189*, 107026. [[CrossRef](#)]
6. Sun, M.; Zhao, J.; Pan, Z.; Hu, Q.; Yu, B.; Tan, Y.; Sun, L.; Bai, L.; Wu, C.; Blach, T.P.; et al. Pore characterization of shales: A review of small angle scattering technique. *J. Nat. Gas Sci. Eng.* **2020**, *78*, 103294. [[CrossRef](#)]
7. Zou, C.N.; Zhu, R.K.; Chen, Z.Q.; Ogg, J.G.; Wu, S.T.; Dong, D.Z.; Qin, Z.; Wang, Y.M.; Wang, L.; Lin, S.H.; et al. Organic-matter-rich shales of China. *Earth-Sci. Rev.* **2018**, *189*, 51–78. [[CrossRef](#)]
8. Chen, L.; Zuo, L.; Jiang, Z.X.; Jiang, S.; Liu, K.Y.; Tan, J.Q.; Zhang, L.C. Mechanisms of shale gas adsorption: Evidence from thermodynamics and kinetics study of methane adsorption on shale. *Chem. Eng. J.* **2019**, *361*, 559–570. [[CrossRef](#)]

9. Chen, L.; Jiang, Z.X.; Liu, Q.X.; Jiang, S.; Liu, K.Y.; Tan, J.Q.; Gao, F.L. Mechanism of shale gas occurrence: Insights from comparative study on pore structures of marine and lacustrine shales. *Mar. Pet. Geol.* **2019**, *104*, 200–216. [[CrossRef](#)]
10. Fan, J.X.; Michael, J.M.; Chen, X.; Wang, Y.; Zhang, Y.D.; Chen, Q.; Chi, Z.L.; Chen, F. Biostratigraphy of Black Graptolite Shales from the Ordovician-Silurian Longmaxi Formation in South China. *Earth Sci.* **2012**, *42*, 130–139. [[CrossRef](#)]
11. Ma, S.M.; Zou, X.Y.; Zhu, Y.M.; Li, X.Q.; Zhao, P. Study on the relationship between graptolite and shale gas origin of Longmaxi Formation in southern Sichuan. *Coal Sci. Technol.* **2015**, *43*, 106–109. [[CrossRef](#)]
12. Wang, Y.M.; Dong, D.Z.; Li, X.J.; Huang, J.L.; Wang, S.F.; Wu, W. Stratigraphic sequence and sedimentary characteristics of Lower Silurian Longmaxi Formation in the Sichuan Basin and its peripheral areas. *Nat. Gas Ind. B* **2015**, *2*, 222–232. [[CrossRef](#)]
13. Chen, X.; Fan, J.X.; Zhang, Y.D.; Wang, H.Y.; Chen, Q.; Wang, W.H.; Liang, F.; Guo, W.; Zhao, Q.; Nie, H.K.; et al. Division and delineation of Wufeng and Longmaxi Black shales in the Yangtze overlying area. *J. Stratigr.* **2015**, *39*, 351–358. [[CrossRef](#)]
14. Zou, C.N.; Gong, J.M.; Wang, H.Y.; Shi, Z.S. Importance of graptolite evolution and biostratigraphic calibration on shale gas exploration. *China Pet. Explor.* **2019**, *24*, 1–6. [[CrossRef](#)]
15. Mu, E.Z. A study of Graptolites in China. *Acta Palaeontol. Sin.* **1980**, 84–92. [[CrossRef](#)]
16. Wang, H.Y.; Guo, W.; Liang, F.; Zhao, Q. Biostratigraphy characteristics and scientific meaning of the Wufeng and Longmaxi Formation black shales at well Wei 202 of the Weiyuan shale gas field, Sichuan Basin. *J. Stratigr.* **2015**, *39*, 289–293. [[CrossRef](#)]
17. Wang, H.Y.; Guo, W.; Liang, F.; Zhao, Q.; Liu, D.X.; Zhou, J.; Du, D.; Pi, S.H. Black shale biostratigraphic characteristics and stratigraphic correlation in the Wufeng and Longmaxi Fms of the Xuanhan–Wuxi areas. *Nat. Gas Ind.* **2017**, *37*, 27–33. [[CrossRef](#)]
18. Chen, X.; Fan, J.X.; Wang, W.H.; Wang, H.Y.; Nie, H.K.; Shi, X.W.; Wen, Z.D.; Chen, D.Y.; Li, W.J. Stage-progressive distribution pattern of the Longmaxi black graptolitic shales from Guizhou to Chongqing, Central China. *Sci. China Earth Sci.* **2017**, *47*, 720–732. [[CrossRef](#)]
19. Chen, X.; Chen, Q.; Zhen, Y.Y.; Wang, H.Y.; Zhang, L.N.; Zhang, J.P.; Wang, W.H.; Xiao, Z.H. Circumjacent distribution pattern of the Longmaxi graptolitic black shale (early Silurian) on the Yichang Uplift and its peripheral region. *Sci. China Earth Sci.* **2018**, *48*, 1198–1206. [[CrossRef](#)]
20. Finney, S.C.; Berry, W.B.N. New perspectives on graptolite distributions and their use as indicators of platform margin dynamics. *Geology* **1997**, *25*, 919–922. [[CrossRef](#)]
21. Machel, H.G. Bacterial and thermochemical sulfate reduction in diagenetic settings—old and new insights. *Sediment. Geol.* **2001**, *140*, 143–175. [[CrossRef](#)]
22. Raiswell, R.; Berner, R.A. Pyrite formation in euxinic and semi-euxinic sediments. *Am. J. Sci.* **1985**, *285*, 710–724. [[CrossRef](#)]
23. Riciputi, L.R.; Cole, D.R.; Machel, H.G. Sulfide formation in reservoir carbonates of the Devonian Nisku Formation, Alberta, Canada: An ion microprobe study. *Geochim. Cosmochim. Acta* **1996**, *60*, 325–336. [[CrossRef](#)]
24. Zhang, J.; Liang, H.D.; He, X.Q.; Yang, Y.; Chen, B.H. Sulfur isotopes of framboidal pyrite in the Permian-Triassic boundary clay at Meishan section. *Acta Geol. Sin.* **2011**, *85*, 694–701. [[CrossRef](#)]
25. Machel, H.G. *Some Aspects of Diagenetic Sulphate-Hydrocarbon Redox Reactions*; Geological Society, Special Publications: London, UK, 1987; Volume 36, pp. 15–28. [[CrossRef](#)]
26. Krouse, H.R.; Viau, C.A.; Eliuk, L.S.; Ueda, A.; Halas, S. Chemical and isotopic evidence of thermochemical sulphate reduction by light hydrocarbon gases in deep carbonate reservoirs. *Nature* **1988**, *333*, 415–419. [[CrossRef](#)]
27. Gomes, M.L.; Fike, D.A.; Bergmann, K.D.; Jones, C.; Knoll, A.H. Environmental insights from high—Resolution (SIMS) sulfur isotope analyses of sulfides in Proterozoic microbialites with diverse mat textures. *Geobiology* **2018**, *16*, 17–34. [[CrossRef](#)]
28. Nie, H.K.; Jin, Z.J.; Sun, C.X.; He, Z.L.; Liu, G.X.; Liu, Q.Y. The organic matter types of the Wufeng and Longmaxi Formations in the Sichuan Basin, South China: Implications for the formation of organic matter pores. *Energy Fuels* **2019**, *33*, 8076–8100. [[CrossRef](#)]
29. Chen, M.J.; Ning, N.; Hu, G.Y.; Li, J. The hydrocarbon source rocks of Pingliang Formation in western Ordos Basin and its influencing factors. *Chin. Sci. Bull.* **2007**, *S1*, 78–85. [[CrossRef](#)]
30. Sun, Y.P.; Wang, C.G.; Wang, Y.; Yang, W.L.; Xu, H.Z.; Liu, W.B.; Wu, T.H. Geochemical characteristics and exploration potential of Middle Ordovician Pingliang Formation in the Ordos Basin. *Pet. Geol. Exp.* **2008**, *30*, 162–168. [[CrossRef](#)]
31. Wang, Z.W. Geological condition and Favorable Area of Middle-Upper Ordovician Shale Gas in Wuzhong Area. Master’s Thesis, Xi’an University of Petroleum, Shaanxi, China, 2020.
32. Kong, Q.F.; Zhang, W.Z.; Li, J.F.; Wang, K.R. Evaluation of Hydrocarbon Generation Potential of Ordovician Source Rocks on the Western Margin of Ordos Basin. *Nat. Gas Ind.* **2007**, *27*, 62–64. Available online: <http://trqgy.paperonce.org/#/digest?ArticleID=4524> (accessed on 3 November 2022).
33. Zhang, Y.Q.; Guo, Y.R.; Hou, W.; Zhao, Z.Y.; Gao, J.R. Geochemical characteristics and exploration potential of the Middle-Upper Ordovician source rocks on the western and southern margin of Ordos Basin. *Nat. Gas Geosci.* **2013**, *24*, 894–904. [[CrossRef](#)]
34. Fu, S.T.; Fu, J.H.; Huang, Z.L. Geological characteristics of Ordovician marine shale gas in the Ordos Basin and its prospects. *China Pet. Explor.* **2021**, *26*, 33–44. [[CrossRef](#)]
35. Xi, S.L.; Mo, W.L.; Liu, X.S.; Zhang, L.; Li, J.; Huang, Z.L.; Wang, M.; Zhang, C.L.; Zhu, Q.Y.; Yan, Y.; et al. Shale gas exploration potential of Ordovician Wulalike Formation in the western margin of Ordos Basin: Case study of Well Zhongping 1. *Nat. Gas Geosci.* **2021**, *32*, 1235–1246. [[CrossRef](#)]
36. Wu, D.X.; Wu, X.N.; Li, C.S.; Yu, Z.; Li, W.L.; Cai, J.; Li, G.J. Sedimentary model and hydrocarbon-generation potential of source rock of the Ordovician Ulalik Formation in western Ordos Basin. *Mar. Orig. Pet. Geol.* **2021**, *26*, 123–130. [[CrossRef](#)]

37. Zhang, C.G. Forming Evolution and Sediments Accumulation & Distribution Regularity of Central Paleouplift in Eopaleozoic, Ordos Basin. Ph.D. Thesis, Chengdu University of Technology, Sichuan, China, 2020.
38. Goodarzi, F.; Eckstrand, O.R.; Snowdon, L.; Williamson, B.; Stasiuk, L.D. Thermal metamorphism of bitumen in Archean rocks by ultramafic volcanic flows. *Int. J. Coal Geol.* **1992**, *20*, 165–178. [[CrossRef](#)]
39. Goodarzi, F.; Norford, B.S. Variation of graptolite reflectance with depth of burial. *Int. J. Coal Geol.* **1989**, *11*, 127–141. [[CrossRef](#)]
40. Bertrand, R. Correlations among the reflectances of vitrinite, chitinozoans, graptolites and scolecodonts. *Org. Geochem.* **1990**, *15*, 565–574. [[CrossRef](#)]
41. Fan, Y.P.; Liu, Y.; Wen, Z.G.; Wang, Z.X.; Zhang, Y.L.; Tang, P.H.; Xu, Y.H.; Tian, Y.J.; Chen, J.; Yan, G. Characteristics of Thermal Maturity of Graptolite-Bearing Shales in Wufeng-Longmaxi Formations on Northern Margin of Xuefeng Mountain. *Earth Sci.* **2019**, *44*, 3725–3735. [[CrossRef](#)]
42. Wang, Y.; Qiu, N.S.; Yang, Y.F.; Rui, X.Q.; Zhou, Y.Y.; Fang, G.J.; Wu, H.; Shen, B.J.; Cheng, L.J. Thermal Maturity of Wufeng-Longmaxi Shale in Sichuan Basin. *Earth Sci.* **2019**, *44*, 953–971. [[CrossRef](#)]
43. Luo, Q.Y.; Hao, J.Y.; Skovsted, C.B.; Luo, P.; Khan, I.; Wu, J.; Zhong, N.N. The organic petrology of graptolites and maturity assessment of the Wufeng-Longmaxi Formations from Chongqing, China: Insights from reflectance cross-plot analysis. *Int. J. Coal Geol.* **2017**, *183*, 161–173. [[CrossRef](#)]
44. Luo, Q.Y.; Hao, J.Y.; Skovsted, C.B.; Xu, Y.H.; Liu, Y.; Jin, W.; Zhang, S.N.; Wang, W.L. Optical characteristics of graptolite-bearing sediments and its implication for thermal maturity assessment. *Int. J. Coal Geol.* **2018**, *195*, 386–401. [[CrossRef](#)]
45. Petersen, H.I.; Schovsbo, N.H.; Nielsen, A.T. Reflectance measurements of zooclasts and solid bitumen in Lower Paleozoic shales, southern Scandinavia: Correlation to vitrinite reflectance. *Int. J. Coal Geol.* **2013**, *114*, 1–18. [[CrossRef](#)]
46. Luo, Q.Y.; Hao, J.Y.; Li, K.W.; Dai, N.; Luan, J.H.; Cheng, L.J.; Zhang, Z.P.; Hu, K.; Zhong, N.N. The optical characteristics of the graptolites in the Wufeng-Longmaxi Formations and its application for the thermal maturity evaluation. *Nat. Gas Geosci.* **2017**, *28*, 1855–1863. [[CrossRef](#)]
47. Chen, X.; Zhang, Y.D.; Daniel, G.; Stig, M.B.; Fan, J.X.; Wang, Z.H.; Stanley, C.F.; Chen, Q.; Ma, H. *Darriwilian to Katian (Ordovician) Graptolites from Northwest China*; Wu, X.F., Ed.; Zhejiang University Press: Hangzhou, China, 2018; pp. 83–293.
48. Ma, Y.; Zhong, N.N.; Cheng, L.J.; Pan, Z.J.; Dai, N.; Zhang, Y.; Yang, L. Pore structure of the graptolite-derived OM in the Longmaxi Shale, southeastern Upper Yangtze Region, China. *Mar. Pet. Geol.* **2016**, *72*, 1–11. [[CrossRef](#)]
49. Luo, Q.Y.; Zhong, N.N.; Dai, N.; Zhang, W. Graptolite-derived organic matter in the wufeng-longmaxi Formations (upper Ordovician-lower Silurian) of southeastern Chongqing, China: Implications for gas shale evaluation. *Int. J. Coal Geol.* **2016**, *153*, 87–98. [[CrossRef](#)]
50. Zhao, D.F. Quantitative Characterization of Pore Structure of Shale Reservoirs in the Lower Paleozoic Wufeng-Longmaxi Formation of the East Sichuan Area. Ph.D. Thesis, China University of Mining and Technology, Jiangsu, China, 2020.
51. Zhao, H.G.; Liu, C.Y.; Wang, F.; Wang, J.Q. Structural division and characteristics in the western edge of Ordos Basin. *Oil Gas Geol.* **2016**, *27*, 173–179. [[CrossRef](#)]
52. Li, W.H.; Chen, Q.; Li, Z.C.; Wang, R.G.; Wang, Y.; Ma, Y. Lithofacies Palaeogeography of Early Paleozoic in Ordos Area. *J. Palaeogeogr.* **2012**, *14*, 85–100+3.
53. Zhao, Z.Y.; Sun, Y.S.; Li, C.S.; Zhang, Q. Stratigraphic Division and Correlation of Ordovician System in Ordos Basin. *Spec. Oil Gas Reserv.* **2015**, *22*, 9–17. [[CrossRef](#)]
54. Ni, C.H.; Zhou, X.J.; Wang, G.S.; Yang, F.; Liu, Y.L. Characteristics and hydrocarbon generation evolution of Pingliang Formation source rocks, southern Ordos Basin. *Pet. Geol. Exp.* **2010**, *32*, 572–577. [[CrossRef](#)]
55. Liu, Q.Y.; Jin, Z.J.; Wang, Y.; Han, P.L.; Tao, Y.; Wang, Q.Z.; Ren, Z.L.; Li, W.H. Gas filling pattern in Paleozoic marine carbonate reservoir of Ordos Basin. *Acta Petrol. Sin.* **2012**, *28*, 847–858. Available online: http://www.ysxb.ac.cn/article/id/aps_20120313 (accessed on 3 November 2022).
56. Deng, K.; Zhou, W.; Deng, H.C.; Chen, W.L. Geological conditions of shale gas enrichment in Pingliang Formation, Ordos Basin. *J. Chengdu Univ. Technol. (Sci. Technol. Ed.)* **2013**, *40*, 595–602. [[CrossRef](#)]
57. Wang, C.G.; Wang, Y.; Xu, H.Z.; Sun, Y.P.; Yang, W.L. Discussion on the evolution of source rocks in Lower Paleozoic of Ordos Basin. *Acta Petrol Sin.* **2009**, *30*, 38–45+50. [[CrossRef](#)]
58. Zhang, T.B. The Transition of Tectonic-Sedimentary Framework and Its Geological Significance in the Late Early Paleozoic in the Southern Ordos Basin. MA Thesis, Northwest University, Shannxi, China, 2021.
59. Goodarzi, F.; Norford, B.S. Optical Properties of Graptolite Epiderm a Review. *Bull. Geol. Soc. Den.* **1986**, *35*, 141–147. [[CrossRef](#)]
60. Cao, C.Q.; Shang, Q.H.; Fang, Y.T. Explore the graptolite reflectivity of the Ordovician, Silurian hydrocarbon source rock maturity instructions. *Acta Palaeontol. Sin.* **2000**, *39*, 151–156. [[CrossRef](#)]
61. Zhang, D.D.; Liu, W.H.; Wang, X.F.; Luo, H.Y.; Wang, Q.T.; Li, Y.N.; Li, F.J. Genetic types and characteristics of deep oil and gas plays. *Oil Gas Geol.* **2021**, *42*, 1169–1180. [[CrossRef](#)]
62. Sun, M.Z.; Meng, Q.X.; Zheng, J.J.; Wang, G.C.; Fang, X.; Wang, Z.D. Analysis of organic acid salts of marine carbonate rocks in Tarim Basin. *J. Cent. South Univ. Sci. Technol.* **2013**, *44*, 216–222. [[CrossRef](#)]
63. Wu, T.H.; Guan, P.; Liu, W.H. Organic acid salt as the possible hydrocarbon source matter in carbonate rocks. *Nat. Gas Ind.* **2005**, *25*, 11–13+17. [[CrossRef](#)]
64. Liu, W.H.; Wang, J.; Tengre, Q.; Qin, J.Z.; Ran, D.; Tao, C.; Lu, L.F. Multiple hydrocarbon generation of marine strata and its tracer technique in China. *Acta Pet. Sin.* **2012**, *33*, 115–125. [[CrossRef](#)]

65. Liu, P.; Wang, X.F.; Fang, X.; Zheng, J.J.; Li, X.F.; Meng, Q. A New Method to Measure the Value of Organic Abundance in Carbonate Rocks. *Acta Sedimentol. Sin.* **2016**, *34*, 200–206. [[CrossRef](#)]
66. Liu, W.H.; Hu, G.; Tenger, Wang, J.; Lu, L.F.; Xie, X.M. Organism assemblages in the Paleozoic source rocks and their implications. *Oil Gas Geol.* **2016**, *37*, 617–626. [[CrossRef](#)]
67. Zhu, Y.M.; Zhang, H.; Kang, W.; Wang, Y.; Chen, S.B. Organic nanopores of Longmaxi and Qiongzhusi Formations in the Upper Yangtze: Biological precursor and pore network. *Nat. Gas Geosci.* **2015**, *26*, 1507–1515. [[CrossRef](#)]
68. Borjigin, T.; Shen, B.J.; Yu, L.J.; Yang, Y.F.; Zhang, W.T.; Tao, C.; Xi, B.B.; Zhang, Q.Z.; Bao, F.; Qin, J.Z. Mechanisms of shale gas generation and accumulation in the Ordovician Wufeng-Longmaxi Formation, Sichuan Basin, SW China. *Pet. Explor. Dev.* **2017**, *44*, 69–78. [[CrossRef](#)]
69. Li, G.; Zhao, D.F.; Guo, Y.H. The relationship between graptolite of Longmaxi shale and sedimentary environment in southeastern Sichuan. *Sci. Technol. Eng.* **2018**, *18*, 16–23. [[CrossRef](#)]
70. Berry, W.; Boucot, A.J. Glacio-Eustatic Control of Late Ordovician-Early Silurian Platform Sedimentation and Faunal Changes. *GSA Bull.* **1973**, *84*, 275–284. [[CrossRef](#)]
71. Chen, X. Graptolite Depth Zonation. *Acta Palaeontol. Sin.* **1990**, *5*, 507–526. [[CrossRef](#)]
72. Boucot, A.J.; Chen, X. Fossil Plankton Depth Zones. *Palaeoworld* **2009**, *18*, 213–234. [[CrossRef](#)]
73. Zhu, G.Y.; Zhang, S.C.; Liang, Y.B.; Dai, J.X.; Li, J. Isotopic Evidence of TSR Origin of High H₂S Bearing Natural Gas in Feixianguan Formation in Northeast Sichuan. *Sci. China Ser. D Earth Sci.* **2005**, 1037–1046. [[CrossRef](#)]
74. Shao, D.B.; Bao, H.P.; Wei, L.B.; Cai, Z.H.; Wu, C.Y.; Zhou, L.X.; Cao, Y.G. Tectonic palaeogeography evolution and sedimentary filling characteristics of the Ordovician in the Ordos area. *J. Palaeogr.* **2019**, *21*, 537–556. [[CrossRef](#)]
75. Yu, Z.; Zhou, G.J.; Li, C.S.; Song, X.J.; Luo, C.; Wu, X.N.; Wu, D.X.; Hu, Z. Tectonic-lithofacies paleogeographic characteristics of Ordovician Kelimoli and Wulalike stages in the western edge of Ordos Basin. *Nat. Gas Geosci.* **2021**, *32*, 816–825. [[CrossRef](#)]